Available online at www.sciencedirect.com
ScienceDirect
European Journal of Pharmaceutics and Biopharmaceutics 69 (2008) 454–465
European Journal of Pharmaceutics and Biopharmaceutics
www.elsevier.com/locate/ejpb

Research paper

Preparation, characterization and in vivo evaluation of amorphous atorvastatin calcium nanoparticles using supercritical antisolvent (SAS) process

Min-Soo Kim [a,1], Shun-Ji Jin [a,1], Jeong-Soo Kim [a], Hee Jun Park [a], Ha-Seung Song [a], Reinhard H.H. Neubert [b], Sung-Joo Hwang [a,*]

[a] *Chungnam National University, Daejeon, Republic of Korea*
[b] *Martin Luther University, Halle–Wittenberg, Germany*

Received 23 October 2007; accepted in revised form 4 January 2008
Available online 18 January 2008

Abstract

In this work, amorphous atorvastatin calcium nanoparticles were successfully prepared using the supercritical antisolvent (SAS) process. The effect of process variables on particle size and distribution of atorvastatin calcium during particle formation was investigated. Solid state characterization, solubility, intrinsic dissolution, powder dissolution studies and pharmacokinetic study in rats were performed. Spherical particles with mean particle size ranging between 152 and 863 nm were obtained by varying process parameters such as precipitation vessel pressure and temperature, drug solution concentration and feed rate ratio of CO_2/drug solution. XRD, TGA, FT-IR, FT-Raman, NMR and HPLC analysis indicated that atorvastatin calcium existed as anhydrous amorphous form and no degradation occurred after SAS process. When compared with crystalline form (unprocessed drug), amorphous atorvastatin calcium nanoparticles were of better performance in solubility and intrinsic dissolution rate, resulting in higher solubility and faster dissolution rate. In addition, intrinsic dissolution rate showed a good correlation with the solubility. The dissolution rates of amorphous atorvastatin calcium nanoparticles were highly increased in comparison with unprocessed drug by the enhancement of intrinsic dissolution rate and the reduction of particle size resulting in an increased specific surface area. The absorption of atorvastatin calcium after oral administration of amorphous atorvastatin calcium nanoparticles to rats was markedly increased.

Keywords: Atorvastatin calcium; Supercritical antisolvent; Nanoparticle; Amorphous form

1. Introduction

Atorvastatin is a selective, competitive inhibitor of HMG-CoA reductase and is commonly used as atorvastatin calcium. Atorvastatin calcium is [R-(R*,R*)]-2-(4-fluorophenyl)-β,δ-dihydroxy-5-(1-methylethyl)-3-phenyl-4-[(phenylamino)carbonyl]-1*H*-pyrrole-1-heptanoic acid, calcium salt (2:1) trihydrate. Atorvastatin calcium is a white to off-white crystalline powder that is insoluble in aqueous solutions of pH 4 and below, which are the conditions typically present in the stomach of a subject. Atorvastatin calcium is very slightly soluble in distilled water, pH 7.4 phosphate buffer and acetonitrile, slightly soluble in ethanol, and freely soluble in methanol [1]. Atorvastatin is rapidly absorbed after oral administration, with time to reach peak concentrations (T_{max}) within 1–2 h. The fraction absorbed (%) and absolute bioavailability of atorvastatin are approximately 30% and 12%, respectively [2]. The low systemic availability is attributed to presystemic clearance in gastrointestinal mucosa and/or hepatic first-pass metabolism [2–4]. Recently, Shen and Zhong [5] showed that the use of SMEDDS for delivery

* Corresponding author. National Research Laboratory of Pharmaceutical Technology, College of Pharmacy, Chungnam National University, 220 Gung-dong, Yuseong-gu, Daejeon 305-764, Republic of Korea. Tel.: +82 42 821 5922; fax: +82 42 823 3078.
E-mail address: sjhwang@cnu.ac.kr (S.-J. Hwang).
[1] These authors equally contributed in this study as first author.

0939-6411/$ - see front matter © 2008 Elsevier B.V. All rights reserved.
doi:10.1016/j.ejpb.2008.01.007

of atorvastatin could improve its solubility and permeability through mucous membrane significantly.

Recently, micro- and nano-particle formation processes based on the use of supercritical fluids as solvents or anti-solvents for poorly water soluble active pharmaceutical ingredients (APIs) have been introduced as a viable means of controlling particle formation to improve physicochemical properties in solid state. Supercritical CO_2 (SC-CO_2) is the most widely used supercritical fluid because of its mild critical conditions ($T_c = 31.1$ °C, $P_c = 7.38$ MPa), non-toxicity, non-flammability and low price [6]. The pharmaceutical applications of supercritical fluid technology using carbon dioxide enable to modify the solid state properties of APIs, such as characteristics of particles (size, shape, surface, crystal structure and morphology), crystallinity and polymorphism affecting their dissolution rate and bioavailability [7–11]. Many researchers have employed supercritical fluid techniques for micronization and for recrystallization of various APIs [12,13]. In addition, the modification of solid state characteristics, such as crystal habit, crystallinity and polymorphism, has been successfully achieved through the recrystallization of drug particles using various SAS processes [14–17].

Our research aimed to improve the bioavailability of atorvastatin calcium by modification of its solid state properties using SAS process. In this study, the effect of process variables on particle size and distribution of atorvastatin calcium during particle formation was investigated. Their physicochemical properties in the solid state were characterized by powder X-ray diffraction (XRD), thermal gravimetric analysis (TGA), Fourier transform infrared (FT-IR) spectroscopy and Fourier transform Raman (FT-Raman) spectroscopy. Solubility, intrinsic dissolution and pharmacokinetic studies in rats were also performed to compare the physicochemical and absorption properties of crystalline form (unprocessed drug) and amorphous form (SAS processed drug).

2. Materials and methods

2.1. Materials

Atorvastatin calcium trihydrate (Form I) was obtained from Zhejiang Jiangbei Pharmaceutic (China). Carbon dioxide (CO_2) with high purity of 99.9% was supplied from Hanmi Gas Co. Ltd. (South Korea). All organic solvents were of high performance liquid chromatography (HPLC) grade. All other chemicals were of reagent grade.

2.2. SAS process

The SAS process was performed using the experimental equipment, as shown in Fig. 1. First, atorvastatin calcium was dissolved in methanol. Then, CO_2 from a storage tank was delivered into the top of the particle precipitation vessel (approximately 1.9 L) through the outer capillary of the two-flow spray nozzle at a constant rate using a homemade plunger pump until the desired pressure was obtained. Once the pressure and temperature had equilibrated, the drug solution was co-introduced into the particle precipitation vessel by a HPLC liquid pump (Model 307, Gilson Inc., USA) with SC-CO_2 through the inner capillary of the two-flow spray nozzle. The residual solvent (SC-CO_2 and methanol) was drained out of the particle precipitation vessel by the backpressure regulator (Tescom, model 26-1723-24-194). At washing step, an additional SC-CO_2 continued to flow into the precipitation vessel for further 1 h to wash out the residual content of methanol solubilized in the supercritical antisolvent. The precipitation vessel was slowly depressurized down to the atmospheric pressure and finally the particles were collected from the internal basket of the precipitation vessel (retained by a 0.1 μm metal frit and paper filter).

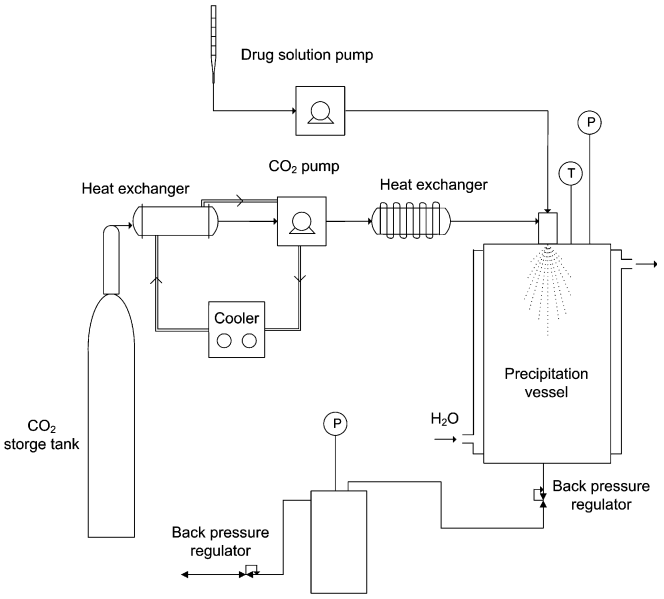

Fig. 1. Schematic diagram of the SAS process.

2.3. Scanning electron microscopy (SEM)

The morphology of particles was examined by scanning electron microscopy (SEM; JSM-6300, Jeol Ltd., Japan).

2.4. Particle size analysis

The particle size and particle size distribution of samples were determined by dynamic light scattering (DLS) using electrophoretic light scattering spectrophotometer (ELS-8000, Otsuka Electronics, Japan). The samples were dispersed in mineral oil (Macrol 52, Exxon Mobil Co., USA) and sonicated for 10 min at 120 W (Branson 8210, Branson Ul-trasonics Co., Danbury, CT, USA). Analyzing the DLS data using the cumulant method, we obtained the information about particle size. The particle size distribution was also estimated from the correlation function

profile using histogram analysis. The particle size analysis of samples was also measured from SEM images using ITPro 3.03 image analysis software (Sometech Inc., Korea). About 500 particle diameters were considered in each particle size distribution. Geometric mean diameter and standard deviation based on number of particles were calculated using OriginPro 7.5 Software (OriginLab Co., USA) and then they were converted to geometric volume-number mean diameter using Hatch–Choate equation [18].

2.5. Powder X-ray diffraction (XRD)

Powder X-ray diffraction patterns were recorded on a Rigaku Powder X-ray diffraction system, Model D/MAX-2200 Ultima/PC (Japan) with Ni-filtered Cu-Kα radiation. The samples were run over the most informative range from 5° to 60° of 2θ. The step scan mode was performed with a step size of 0.02° at a rate of 3°/min.

2.6. Thermal gravimetric analysis (TGA)

Thermal gravimetric analysis (TGA) was performed using a TA instruments (USA) TGA 2950 Thermogravimetrical Analyzer. The experiment was performed with a heating rate of 5 °C/min using nitrogen flow (50 ml/min) and samples were weighed (approximately 5 mg) in open aluminum pans and the percentage weight loss of the samples was monitored from 20 to 300 °C.

2.7. Head space GC analysis

Analysis of the residual solvents was carried out on an Agilent 6890 gas chromatograph (Agilent Technologies, USA) equipped with a flame ionization detection (FID) system. A DB-5 capillary column (30 m × 0.32 mm i.d.; film thickness 0.25 μm) was used. GC conditions used were: oven temperature of 40 °C for 8 min. The injector was maintained at 180 °C (split mode, ratio 1:1) and helium was used as the carrier gas (7 ml/min). Head space samples were prepared in 10 ml vials filled by 10 ml of water in which 20 mg of drug was dispersed. The head space conditions were: equilibration time 30 min at 100 °C; pressurization time 2 min; loop fill time 1 min.

2.8. BET analysis

The specific surface area of samples was determined by N_2 adsorption using Surface Area Analyzer ASAP 2010 (Micromeritics Instrument Corporation, USA).

2.9. NMR analysis

A quantity of atorvastatin calcium (approximately 10 mg/ml) was dissolved in denaturized methanol. ^1H nuclear magnetic resonance (NMR) spectra were obtained with JEOL JNM-AL400 instrument (Akishima, Japan) with a 5 mm auto tune probe, operating at 400 MHz at 25 °C. Chemical shifts were given as parts per million (ppm) downfield from that of an external standard, tetramethylsilane.

2.10. Fourier transform infrared (FT-IR) spectroscopy

FT-IR spectra were obtained on a FT-IR spectrometer (Bruker FT-IR: Tensor 27, Germany) using attenuated total reflectance method. The scanning range was 650–4000 cm^{-1} and the resolution was 4 cm^{-1}. Number of reference scans was 64.

2.11. Fourier transform Raman (FT-Raman) spectroscopy

FT-Raman spectra were obtained using a FT-Raman spectrometer RFS 100/S (Bruker Optics, Germany) equipped with a Nd:YAG Laser with an excitation wavelength of 1064 nm. The samples were prepared in an aluminum pan and the laser was directly turned on the sample's surface. The Raman laser power was 500 mW. For each spectrum 200 scans were averaged. The resolution was 4 cm^{-1}, the apodization function Blackman–Harris-4-term and the phase resolution 128.

2.12. Solubility studies

For kinetic solubility studies, excess solid (approximately 100 mg of atorvastatin) was placed with 200 ml water in a water-jacketed vessel linked to a temperature controlled water bath held at 37 ± 0.1 °C. Solutions were agitated constantly by overhead stirrers at 200 rpm. Suitable aliquots were withdrawn in certain time intervals and filtered using a 0.11 μm nylon syringe filter. Filtered samples were diluted with methanol, and the concentration of atorvastatin was determined by HPLC. In addition, saturation solubility of atorvastatin calcium was determined in water with different concentration of SLS (0–1 w/v%). The samples placed on a shaking water bath were shaken (60 rpm) at 37 ± 0.1 °C for 24 h previously determined to be adequate time for equilibration. Suitable aliquots were withdrawn in certain time intervals and filtered using a 0.11 μm nylon syringe filter. The filtrate was diluted with methanol, and the concentration of atorvastatin was determined by HPLC. Chromatographic analyses were performed on a Waters HPLC system consisting of a pump (Model 600), an auto-sampler (Model 717 plus), and a UV detector (Model 486 Tunable Absorbance Detector). The C_{18} reverse phase column (Xterra, 5 μm, 4.6 mm × 250 mm, Waters) was used at room temperature. The mobile phase was composed of a 60:40 mixture of acetonitrile:50 mM sodium acetate in water, where the pH was adjusted to 4.0 with glacial acetic acid. The injection volume was 20 μl, and the eluent flow rate was 1.0 ml/min. The signal was monitored at 245 nm.

2.13. Intrinsic dissolution rate study

Intrinsic dissolution rate (IDR) studies were performed by the stationary disc (0.5 cm^2 surface area, Distek Inc., USA) method using the USP XXVIII paddle method using VK 7000 dissolution testing station and VK 750d heater/circulator (Vankel, USA). Discs were prepared compressing 80 mg of powder (of atorvastatin) in a Perkin Elmer hydraulic press for 1 min under 5 tons compression. Analysis of the compressed discs by DSC and FT-IR confirmed that the crystal form of the original powder was retained following the compression procedure. Intrinsic dissolution rate studies, under sink conditions, were performed in distilled water containing 1% SLS at 37 ± 0.1 °C and 50 rpm. Suitable aliquots were withdrawn in certain time intervals and filtered using a 0.11 μm nylon syringe filter. At each sampling time, an equal volume of the test medium was replaced. Filtered samples were assayed for drug concentration by HPLC.

2.14. Dissolution study

Dissolution studies were performed according to the USP XXVIII paddle method using VK 7000 dissolution testing station and VK 750d heater/circulator (Vankel, USA). The stirring speed used was 50 rpm, and the temperature was maintained at 37 ± 0.1 °C. Each test was carried out in 900 ml of distilled water. Accurately weighted samples containing the equivalent of 10 mg atorvastatin were placed in the dissolution medium. Then, 4 ml of aliquot samples was withdrawn in certain time intervals and filtered using a 0.11 μm nylon syringe filter. At each sampling time, an equal volume of the test medium was replaced. Filtered samples were appropriately diluted with methanol and assayed for drug concentration by HPLC.

2.15. Pharmacokinetic study in rats

Male SD rats (6–7 weeks old) weighing between 180 and 200 g were obtained from Samtaco Bio Korea Inc. (Korea). All rats had free access to tap water and pelleted diet. The rats were housed in a cage and maintained on a 12 h light/dark at room temperature (25 °C) and relative humidity of 55 ± 10%. General and environmental conditions were strictly monitored. All animal experiments were performed according to the "Guidelines for the Care and Use of Laboratory Animals" at Chungnam National University. The rats were deprived of food 24 h before the experiment and food was reoffered 4 h post-dosing. The rats were divided into four groups of five animals each. After anesthesia with diethylether, the femoral artery was cannulated with 23-gauge polyethylene cannula. The cannula was flushed with 0.3 ml of heparin (50 IU) saline solution to prevent blood clotting. After rats recovered from the anesthesia, gelatin minicapsules (Size 9, Torpac, Fairfield, NJ, USA) filled with raw material and SAS processed particles equivalent to 25 mg/kg of atorvastatin, respectively, were administered orally to rats using minicapsule dosing syringe. After administration of the capsules, the rats were immediately given 1 ml of distilled water. Serial blood samples (approximately 300 μl each) were taken via the jugular vein catheter at: predose, 0.5, 1, 1.5, 2, 4, 6, 8 and 12 h post-dosing. Blood samples were held on ice (+4 °C) until centrifuged at 10000 rpm, 4 °C for 10 min. Plasma was transferred to individual Eppendorf tubes and stored at −20 °C until analyzed.

2.16. LC/MS analysis

A plasma sample (100 μl) was spiked with 50 μl of internal standard solution (methaqualone, 100 ng/ml) and 350 μl of acetonitrile was added. After vortex mixing for 30 s, 400 μl of supernatant was carefully transferred to a glass test tube and evaporated to dryness using a centrifugal evaporator (CVE-2000, Eyela, Japan). Then the dried residual was reconstituted in 100 μl of methanol and a 5 μl aliquot was injected into the LC/MS system for the quantification of atorvastatin. The LC/MS system consisted of a LC-10ADvp pump, SIL-10A autoinjector, SPD-10ADvp UV detector, and LCMS-2010A mass spectrometer (Shimadzu, Japan). The mobile phase consisting of 0.1 M ammonium acetate buffer (pH 4.0)/acetonitrile (50:50, v/v) was pumped at a flow rate of 1.0 ml/min. The analytical column was Kromasil C18 (150 × 4.6 mm, 5 μm) and the detection wavelength was 270 nm. The mass spectrometer was operated in positive ion mode and connected to the chromatographic system using an API electrospray interface. The $[M+H]^+$, m/z 251.00 for methaqualone and $[M+H]^+$, m/z 559.00 for atorvastatin were selected as detecting ions, respectively. The MS operating conditions were optimized as follows: drying gas 1.5 l/min, CDL temperature 250 °C, block temperature 200 °C and probe voltage: +4.5 kV. Data processing was performed using the LC/MS solution software (Shimadzu, Japan).

2.17. Pharmacokinetic data analysis

The area under the drug concentration–time curve from zero to 12 h ($AUC_{0\rightarrow 12h}$) and mean residence time (MRT) were calculated using the noncompartmental analysis (WinNonlin 2.1, Pharsight Corp., Mountain View, CA). The maximal plasma concentration of drug (C_{max}) and the time to reach maximum plasma concentration (T_{max}) were directly obtained from plasma data. One-way analysis of variance (ANOVA) test and Tukey's HSD test were performed to demonstrate statistical differences, using SPSS 12.0 software (SPSS, Chicago, IL, USA).

3. Results and discussion

In this study, atorvastatin calcium was precipitated from methanol using SAS process. The operating conditions used in our experiments were selected on the basis of our

previous experiences on the SAS process [19]. The conditions of particle precipitation vessel were investigated at temperature ranging from 40 to 60 °C and pressure ranging from 10 to 18 MPa. The position of the process operating point with respect to the critical point of the mixture CO_2–methanol can have a strong influence on the SAS process [20,21]. Experimental vapor–liquid equilibrium (VLE) data for CO_2–methanol systems showed that in the process conditions with temperatures above 40, 50 and 60 °C, the mixture critical pressures are about 8, 9 and 11 MPa, respectively [22–24]. These operating conditions ensure complete miscibility between the methanol and CO_2. The experimental conditions and mean particle sizes of drug after SAS process are summarized in Table 1. Quantitative measurement of particle size was performed using SEM image analysis and DLS analysis. As shown in Table 1, the mean particle size calculated by cumulant method using DLS measurement was directly comparable to the results of SEM image analysis. The SEM images demonstrate that very small spherical nanoparticles were obtained from SAS process, as compared with unprocessed drug (Fig. 2).

3.1. Effect of process parameters

The particle size and morphology are dominated by two possible mechanisms, evaporation of the solvent into the antisolvent phase and diffusion of the antisolvent into the droplets [25,26]. The density of carbon dioxide, which is influenced by pressure and temperature under supercritical conditions, plays an important role for mass transfer between organic solvents and CO_2 during particle formation [19,27].

The mean particle sizes were somewhat decreased with increasing pressure range from 10 to 18 MPa (40 °C, $R = 90$ and 50 mg/ml) and decreasing temperature range from 40 to 60 °C (12 MPa, $R = 90$ and 50 mg/ml). Experiments above 12 MPa reflected similar results during particle formation using SAS process. Therefore, atorvastatin calcium nanoparticles were prepared at 12 MPa and 40 °C.

The mean particle size of drug precipitated from methanol showed a good linear relation with the density of CO_2, indicating that particle formation is dominated by diffusion of SC-CO_2 into the droplets (methanol + solute) (Fig. 3(b)). Pure carbon dioxide density was obtained from a NIST12 database [28].

The mean particle sizes were somewhat increased with increasing drug concentration. As shown in Fig. 4(a), the mean particle size and distribution of drug precipitated with 25 and 50 mg/ml were similar while the drug precipitated with high drug concentration (150 mg/ml) showed a broader particle size distribution with mean particle sizes of 727 nm. This tendency was also previously reported in the literature [19,29–31] and it can be explained in terms of nucleation and growth processes [32].

Experiments were performed at values of the feed rate ratio ranging between 30 and 120 on a weight basis of CO_2 and drug solution. As shown in Table 1, the mean particle sizes were somewhat increased with increasing the feed rate ratio from 30 to 120. As shown in Fig. 4(b), the mean particle size of drug precipitated from methanol also showed a good linear relation with the mole% of methanol in CO_2. In SAS process, firstly, premixing is created between a fresh drug solution and SC-CO_2, at high supersaturation and predominantly occurs during co-introduction of drug solution and SC-CO_2 into precipitation vessel. This high supersaturation was very important and optimal mole fraction value was observed in terms of product yield and minimum particle size [33]. In this study, the working of the feed rate ratio between drug solution and CO_2 above 90 (below approximately 1 mol% of methanol) was to obtain small mean particle size and narrower particle size distribution. Therefore, the mean particle sizes and distribution of atorvastatin calcium were mainly controlled by the drug concentration, and the feed rate ratio of CO_2 and drug solution.

Table 1
Summary of experiments performed

Run	Pressure (MPa)	Temperature (°C)	Concentration (mg/ml)	Feed rate ratio, R (CO_2/drug solution)	Particle size (nm)	
					SEM[a]	DLS[b]
1	10	40	50	90 (45/0.5)	242	262 ± 61
2	12	40	50	90 (45/0.5)	123	179 ± 50
3	15	40	50	90 (45/0.5)	115	158 ± 41
4	18	40	50	90 (45/0.5)	109	152 ± 47
5	12	50	50	90 (45/0.5)	248	277 ± 65
6	12	60	50	90 (45/0.5)	282	350 ± 31
7	12	40	25	90 (45/0.5)	105	174 ± 48
8	12	40	100	90 (45/0.5)	181	265 ± 80
9	12	40	150	90 (45/0.5)	453	727 ± 224
10	12	40	50	30 (30/1)	504	863 ± 158
11	12	40	50	60 (30/0.5)	238	285 ± 93
12	12	40	50	45 (45/1)	289	401 ± 15
13	12	40	50	60 (60/1)	256	294 ± 43
14	12	40	50	120 (60/0.5)	126	163 ± 30

[a] Geometric volume-number mean diameter.
[b] Mean particle size calculated by cumulant method using dynamic light scattering measurement ($n = 4$, mean ± S.D.).

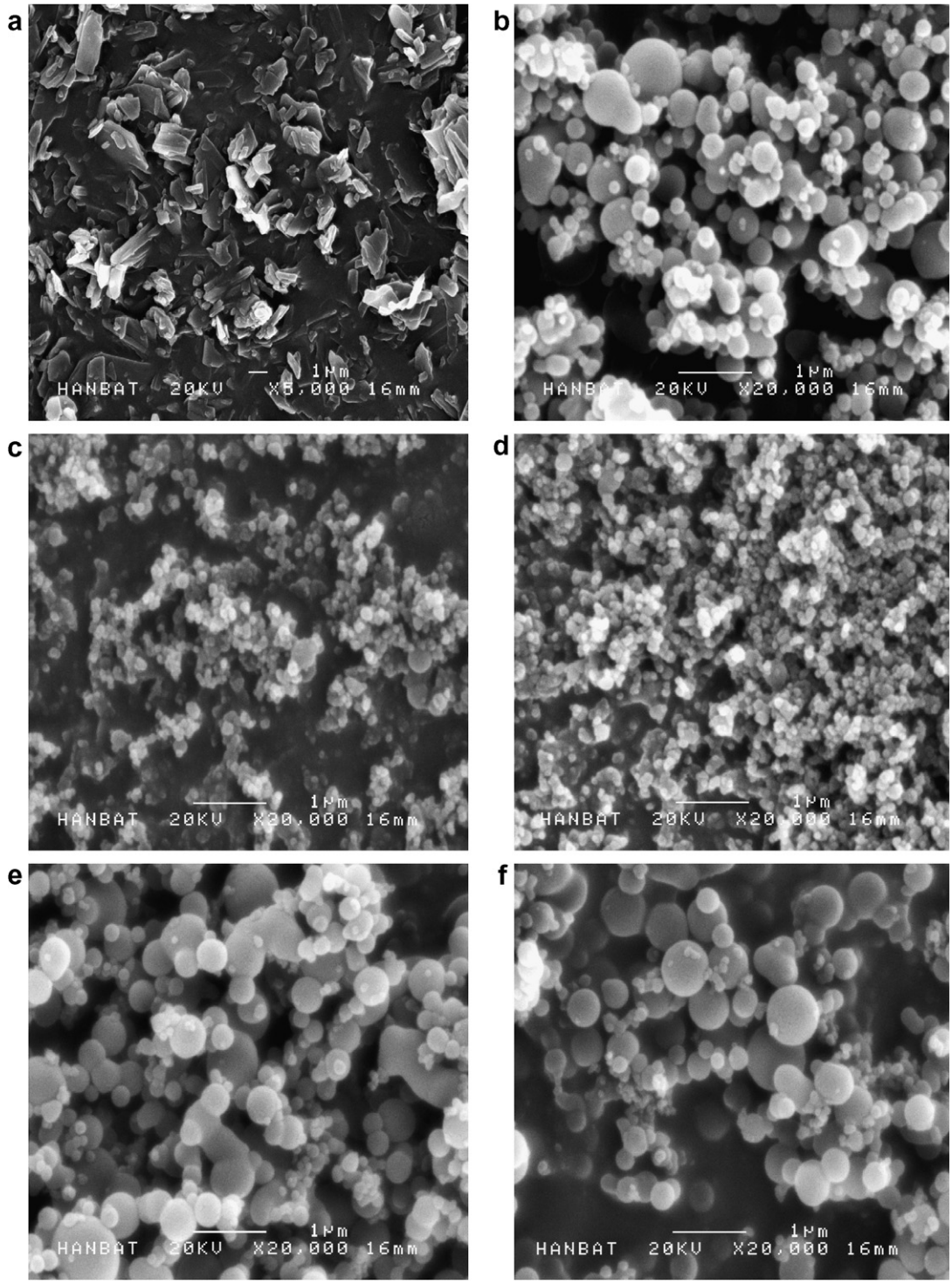

Fig. 2. SEM images of unprocessed atorvastatin calcium (a) and processed atorvastatin calcium precipitated by the SAS process: R1 (b), R2 (c), R3 (d), R5 (e) and R6 (f).

3.2. Solid state characterization

Methanol is the class 2 solvent in the ICH guidelines [34], the amount of residual solvent was severely limited, which is below 3000 ppm (1997). Head space GC analysis revealed that residual methanol was found to be always lower than 50 ppm for all samples in our study. In addition, no chemical degradation of drug was also observed, as confirmed by NMR and HPLC analysis (data not shown). Fig. 5 represents the X-ray diffraction patterns of the atorvastatin calcium before/after SAS process. The diffraction pattern and thermograms of unprocessed drug showed characteristic high-intensity diffraction peaks at 9.12, 9.44, 10.23, 10.54, 11.82, 12.16, 16.97, 19.45, 21.59,

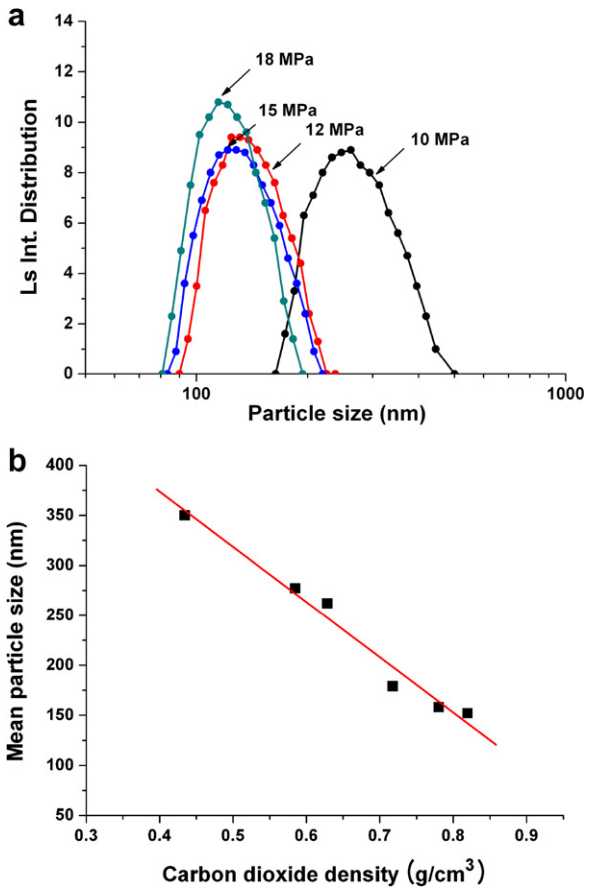

Fig. 3. Influence of pressure (a) and carbon dioxide density (b) on the particle size.

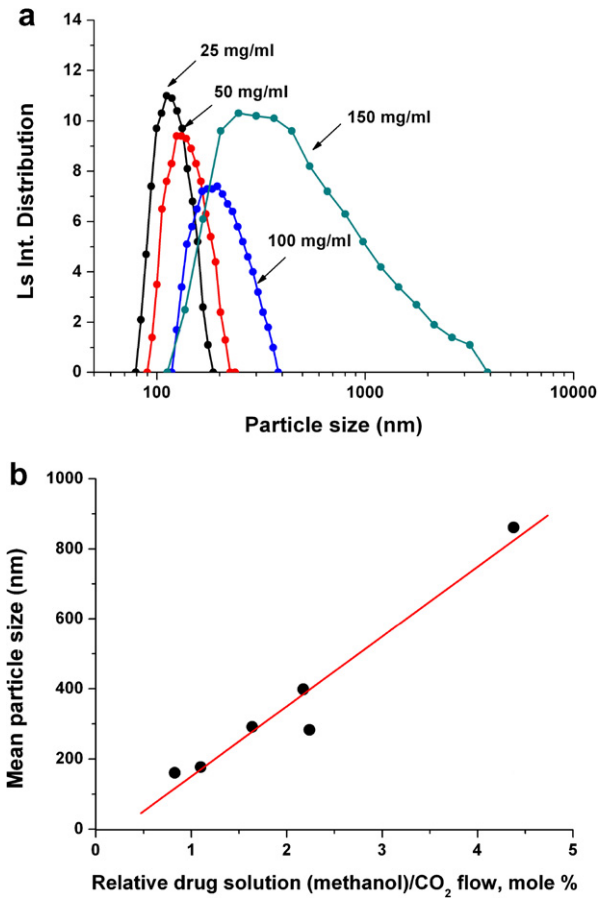

Fig. 4. Influence of drug concentration (a) and the feed rate ratio of CO_2/drug solution (b) on the particle size.

22.62, 23.22 and 23.68° of 2θ. However, no characteristic diffraction peaks corresponding to pure atorvastatin calcium were observed in SAS processed nanoparticles. Therefore, atorvastatin calcium nanoparticles existed as an amorphous form. In addition, while TGA curve of unprocessed drug showed the loss of water indicating trihydrate form (theoretical value of water content of trihydrate, 4.46%), no loss of water was observed in an amorphous atorvastatin calcium nanoparticles, indicating anhydrate form (Fig. 6).

Figs. 7 and 8 show FT-IR and FT-Raman spectra of drug before/after SAS process. The two forms exhibited significant differences in the observed vibrational transitions and the bands in the spectrum of the crystalline form were clearer and sharper than the bands of the amorphous forms. In FT-IR spectra, the most significant peaks (3700–3000 cm^{-1}) were observed in crystalline form (unprocessed drug) due to the stretching of the –OH group associated to a hydrogen bond. While the peak of crystalline form was observed at 3670 cm^{-1} indicating free O–H stretching this peak was not found in FT-IR spectra of amorphous form (SAS processed drug). The 3670 cm^{-1} band probably belongs to the trihydrate functionality. In addition, three bands at about 3361 (N–H stretching), 3222 (asymmetric O–H stretching) and 3055 cm^{-1} (symmetric O–H stretching) were seen in the FT-IR spectra of crystalline form,

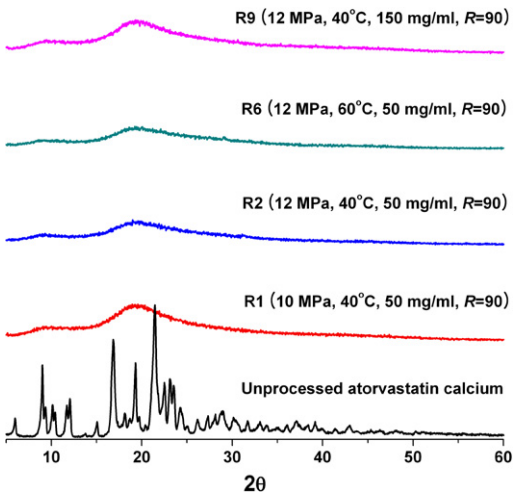

Fig. 5. X-ray diffraction patterns of the drug before/after SAS process.

while broad bands with a shoulder at about 3400, 3320 and 3058 cm^{-1} were observed for FT-IR spectra of amorphous form. In FT-Raman spectra, N–H stretching and O–H stretching vibrations were not only shifted from 3364, 3080 and 3062 cm^{-1} (crystalline form) to 3061 cm^{-1} (amorphous form), but they were also broadened. The CH stretching vibration in the region from 2800 to

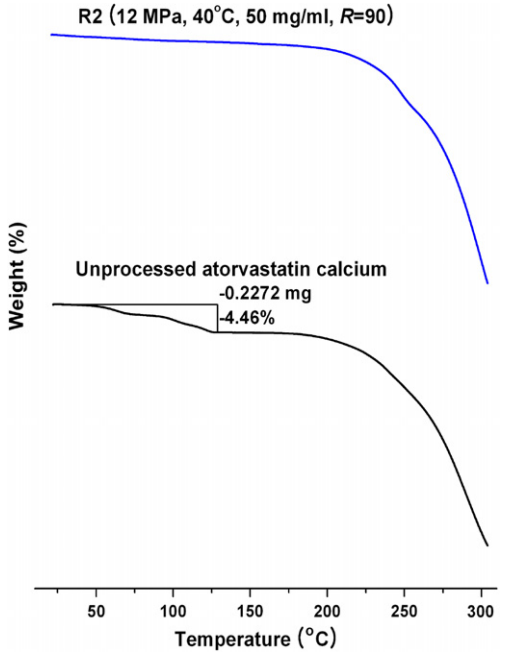

Fig. 6. TGA curves of the drug before/after SAS process.

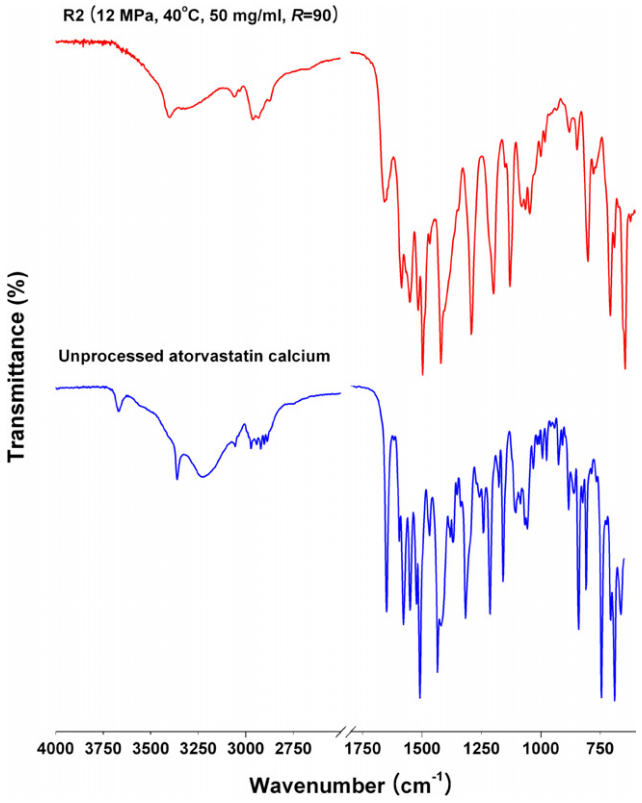

Fig. 7. FT-IR spectra of the drug before/after SAS process.

3000 cm^{-1} the bands of the spectrum of the crystalline form are more pronounced than those of the amorphous form. Furthermore, characteristic bands at about 1649 (asymmetric C=O stretching), 1578 (symmetric C=O stretching), 1550–1468 (four bands related to C–C ring stretching), 1317 (CH_3/CH_2 deformation), 1243 (C–N

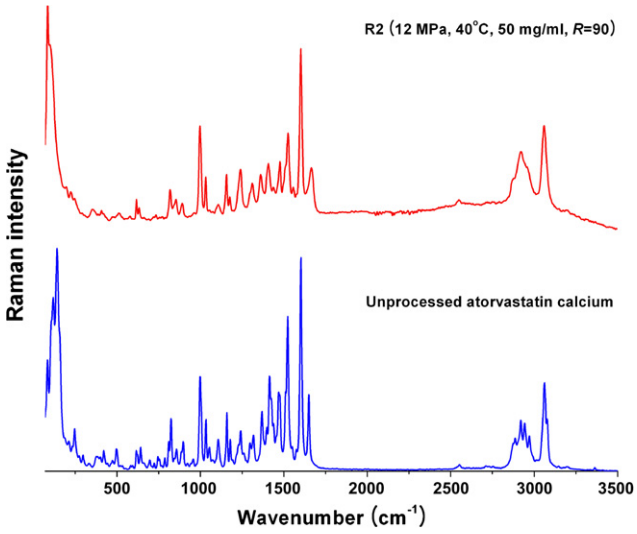

Fig. 8. FT-Raman spectra of the drug before/after SAS process.

stretching) and 1213 cm^{-1} (C–N stretching/C–O stretching) were seen in the FT-IR spectra of crystalline form, while at about 1662, 1594, 1560–1479, 1311 and 1223 cm^{-1} were observed for the FT-IR spectra of amorphous form. Characteristic FT-Raman bands for crystalline form: 1650, 1574, 1551–1475, 1426, 1414, 1397, 1368, 1318, 1262, 1195, 1179, 1159, 1074 and 1053 cm^{-1} and for amorphous form: 1667, 1602, 1557–1478, 1438, 1408, 1361, 1312, 1242, 1177, 1156 and 1107 cm^{-1}. Differences were observed also in the finger print regions in the 1000–70 cm^{-1}. Therefore, FT-IR and FT-Raman spectroscopies were a useful tool to distinguish amorphous form (SAS processed drug) from crystalline form (unprocessed drug).

3.3. Solubility and intrinsic dissolution study

A kinetic solubility study was carried out at 37 °C in water, using the paddle solubility method. As shown in Fig. 9(a), the maximum solubility (approximately 458 μg/ml) was observed in amorphous atorvastatin calcium nanoparticles and then it was gradually decreased. However, the kinetic solubility curve of crystalline form (unprocessed drug) reached the plateau very fast. Amorphous atorvastatin calcium nanoparticles showed characteristic convex solubility curves, suggesting that conversion to crystalline form occurred during the dissolution in water. Nevertheless, a high solubility of atorvastatin, above 300 μg/ml, was maintained for at least 3 h. In fact, partial conversion of amorphous form to crystalline form was confirmed by FT-IR and PXRD of the recovered nanoparticles from solubility studies after 3 h.

Atorvastatin calcium is very slightly soluble in distilled water (143 μg/ml of atorvastatin). For intrinsic dissolution study of atorvastatin, it is inevitable to modify the dissolution medium. Therefore, equilibrium solubility was carried out under different concentration of SLS. Equilibrium

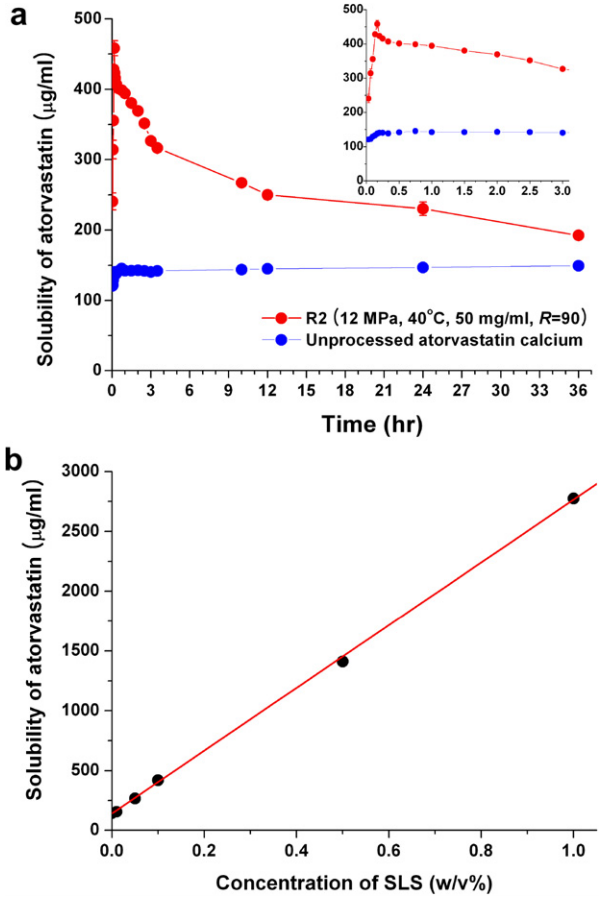

Fig. 9. Kinetic solubility profiles of the drug before/after with SAS process (a) and effect of sodium lauryl sulfate on solubility of atorvastatin calcium (b).

solubility was linearly increased from 2.9-fold (compared with water) at 0.1% SLS to 19.4-fold at 1% SLS as shown in Fig. 9(b). This significant increase was attributed to the micellar solubilization by SLS, considering that the concentrations of SLS examined in this study were well above its critical micelle concentration, 0.008 M or 0.25 w/v% [35]. Intrinsic dissolution studies were performed with distilled water containing 1% SLS under sink condition and until 10% dissolution of initial loading dose, according to USP XXVIII intrinsic dissolution method.

Under sink conditions, the intrinsic dissolution rate J of a solid is given by:

$$J = kC_s \quad (1)$$

where the mass transfer coefficient, $k = D/h$, where D is the diffusivity of the solid and h is the thickness of the diffusion layer which depends on the geometry of the system and of stirring conditions. If the mass transfer coefficient of the drug from the crystalline form (unprocessed drug) and amorphous form (SAS processed drug), under identical hydrodynamic conditions, is assumed to be equal, then Eq. (1) leads to

$$J_A/J_C = C_A/C_C \quad (2)$$

where J_A and J_C are the mass fluxes for amorphous form and crystalline form, respectively, and C_A and C_C are the solubilities of amorphous form and crystalline form, respectively [36]. As shown in Fig. 10(a), the straight lines for the dissolution rates of the two forms had been compared and this revealed that there was a decrease in the slope for amorphous form after 8 min, also the fit of this phase was better than that of the totality of the points. While very good linearity could be observed between all the points for crystalline form (the correlation coefficient varies between 0.9982 and 0.9999), a decrease in the slope could be observed after 8 min for amorphous form. It was always higher than 0.999 if only the points until 8 min were considered. The slopes were calculated from the straight lines until 8 min were increased 3.24-fold as compared with intrinsic dissolution rate of crystalline form (Table 2). From these values, the saturated concentrations of amorphous form were estimated to be approximately 463 μg/ml. This value was similar to the maximum concentration of amorphous form observed in the paddle solubility method, which was 458 μg/ml. After 8 min, the intrinsic dissolution rate of amorphous form was also increased 1.98-fold. In fact, a high solubility of atorvastatin, above 300 μg/ml, was maintained for at least 3 h. Therefore, intrinsic dissolution rate showed a good correlation with

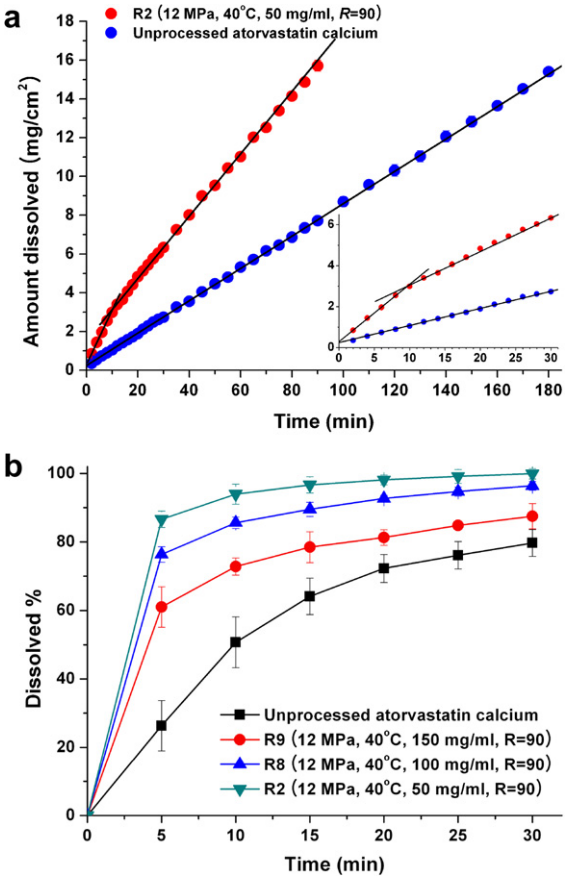

Fig. 10. Intrinsic dissolution profiles (a) and powder dissolution profiles (b) of the drug before/after SAS process.

Table 2
Mean particle size, specific surface area and intrinsic dissolution rate of the drug before/after SAS process

	R2	R8	R9	Unprocessed drug
Mean particle size	179 ± 50 nm[a]	265 ± 80 nm[a]	727 ± 224 nm[a]	3.71 ± 0.18 μm[b]
Specific surface area[c] (m^2/g)	90.28 ± 1.03	47.82 ± 0.51	30.88 ± 0.37	14.55 ± 0.17
Intrinsic dissolution rate[d]	0.279 ± 0.006 (initial phase)	0.280 ± 0.004 (initial phase)	0.280 ± 0.002 (initial phase)	0.086 ± 0.002
(mg/cm^2/min)	0.170 ± 0.004 (second phase)	0.171 ± 0.005 (second phase)	0.171 ± 0.004 (second phase)	

[a] Mean particle size calculated by cumulant method using dynamic light scattering measurement ($n = 4$, mean ± S.D.).
[b] Mean particle size was determined by using a Sympatec laser diffraction analyzer (HELOS/RODOS, Clausthal–Zellerfeld, Germany) consisting of a laser sensor HELOS and a RODOS dry-powder air-dispersion system ($n = 3$, mean ± S.D.).
[c] $n = 3$, mean ± S.D.
[d] $n = 6$, mean ± S.D.

the solubility. Similar to kinetic solubility curves, the intrinsic dissolution profiles suggested that conversion to other phase takes place during the dissolution experiment. To exclude that the conversion of amorphous form to crystalline form did occur at the surface the pellets were withdrawn before the end of some selected dissolution runs. Partial conversion of the amorphous form to crystalline form was confirmed by FT-IR and PXRD of the solid phase collected after intrinsic dissolution test. Nevertheless, the cumulative drug release for amorphous form (SAS processed drug) was always higher than that for crystalline form (unprocessed drug), indicating faster drug release.

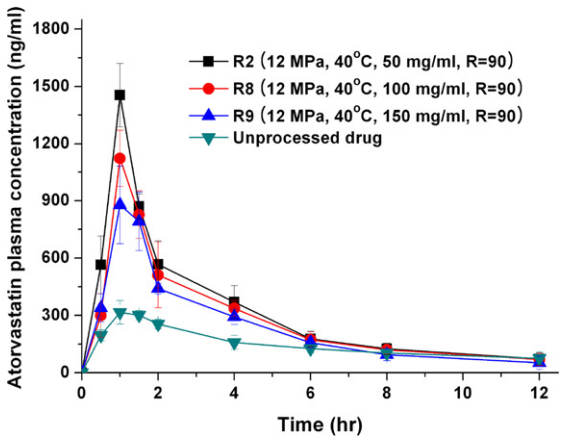

Fig. 11. Plasma concentration time-profile of atorvastatin in rats after oral administration of SAS processed amorphous nanoparticles or unprocessed drug at a dose equivalent to 25 mg of atorvastatin/kg of body weight. Data are expressed as means ± S.D. ($n = 5$).

3.4. Dissolution study and in vivo absorption

Powder dissolution profiles for unprocessed and processed drug precipitated with different drug concentration at 40 °C and 12 MPa, respectively, are shown in Fig. 10(b). The drug was approximately 85% dissolved for processed drug (R2), while only approximately 25% dissolved for unprocessed drug at 5 min. This can be explained by the enhancement of intrinsic dissolution rate and the reduction of particle size resulting in an increased specific surface area. In fact, the processed drug used in dissolution studies had a specific surface area of 90 m^2/g (R2) which was significantly greater than that of unprocessed drug (14 m^2/g). Moreover, the effect of particle size on dissolution profiles was observed between SAS processed samples.

Mean concentration–time profiles of atorvastatin in rats after a single dose (25 mg/kg) of amorphous atorvastatin calcium nanoparticles and crystalline atorvastatin calcium are represented in Fig. 11. The oral absorption of amorphous atorvastatin calcium nanoparticles was obviously higher when compared with crystalline atorvastatin calcium (Table 3). The amorphous nature and small particle size (nano-scale) of API allow for higher apparent solubility, thereby increasing the dissolution rate and increasing the concentration of drug available for absorption [37–39]. As mentioned above, amorphous atorvastatin calcium nanoparticles displayed supersaturation 3.2–3.3 times above the unprocessed drug (crystalline form) and were able to maintain supersaturation for at least 3 h. In vivo data from the current study found that the supersaturating amorphous nanoparticles displayed significantly higher and extended absorption of the API. The analysis of vari-

Table 3
Pharmacokinetic parameters after oral administration of atorvastatin calcium to rats ($n = 5$)

	R2	R8	R9	Unprocessed drug
$AUC_{0\rightarrow 12h}$ (ng h/ml)	3688 ± 269[a,b,c]	3305 ± 136[a,d]	2846 ± 133[a]	1756 ± 101
C_{max} (ng/ml)	1454 ± 166[a,b,c]	1145 ± 107[a]	986 ± 64[a]	334 ± 43
T_{max} (h)	1.0 ± 0	1.1 ± 0.2	1.2 ± 0.3	1.2 ± 0.3
MRT (h)	3.4 ± 0.4[a]	3.6 ± 0.3[a]	3.6 ± 0.3[a]	4.6 ± 0.3

[a] Indicates $P < 0.05$ between unprocessed drug and amorphous nanoparticles.
[b] Indicates $P < 0.05$ between R2 and R8.
[c] Indicates $P < 0.05$ between R2 and R9.
[d] Indicates $P < 0.05$ between R8 and R9.

ance showed that there were significant differences among the samples ($P < 0.05$), which in order of increasing $AUC_{0\rightarrow 12h}$ were ranked by the Student–Newman–Keuls test as follows: unprocessed drug < R9 < R8 < R2. In fact, $AUC_{0\rightarrow 12\,h}$ and C_{max} of atorvastatin were increased with decreasing the particle size. Based on the results from our studies, it was likely that the absorption of atorvastatin was influenced by particle size as well as amorphous nature. The $AUC_{0\rightarrow 12h}$ of the amorphous atorvastatin calcium nanoparticles (179 nm) was 2.1 times that of unprocessed drug, which suggested that it was possible to improve the physicochemical properties and oral absorption of atorvastatin by preparing it as amorphous nanoparticles using the SAS process. Thus, the SAS process for amorphous atorvastatin calcium nanoparticles is a promising method for enhancing their bioavailability.

4. Conclusions

Amorphous atorvastatin calcium nanoparticles, with approximately 152 to 863 nm in mean particle size, were successfully prepared from methanol using SAS process. In particular, the mean particle size of atorvastatin calcium was strongly influenced by the drug concentration and the feed rate ratio of CO_2/drug solution. In addition, XRD, TGA, FT-IR, FT-Raman, NMR and HPLC analysis indicated that atorvastatin calcium existed as anhydrous amorphous form and no degradation occurred after SAS process. When compared with crystalline form (unprocessed drug), amorphous atorvastatin calcium nanoparticles were of better performance in solubility and intrinsic dissolution rate, resulting in higher solubility and faster dissolution rate. In addition, intrinsic dissolution rate showed a good correlation with the solubility. The dissolution rates of amorphous atorvastatin calcium nanoparticles were highly increased in comparison with unprocessed drug by the enhancement of intrinsic dissolution rate and the reduction of particle size, resulting in an increased specific surface area. The absorption of atorvastatin calcium after oral administration of amorphous atorvastatin calcium nanoparticles to rats was markedly increased due to enhanced supersaturation and dissolution properties. Therefore, preliminary results from this study suggested that the preparation of amorphous atorvastatin calcium nanoparticles using SAS process could be a promising approach to improve supersaturation, dissolution and absorption properties of atorvastatin.

Acknowledgments

This work was supported by the Korea Science and Engineering Foundation (KOSEF) through the National Research Laboratory Program funded by the Ministry of Science and Technology (No. M10300000301-06J0000-30110) and by the Energy Conservation Technology Program (2004-E-ID12-P-05-3-010).

References

[1] Physicians' Desk Reference (PDR), electronic version, Thomson PDR, Montvale, NJ (2005).
[2] A. Corsini, S. Bellosta, R. Baetta, R. Fumagalli, R. Paoletti, F. Bernini, New insights into the pharmacodynamic and pharmacokinetic properties of statins, Pharmcol. Ther. 84 (1999) 413–428.
[3] D.D. Cilla, J.L.R. Whitfield, D.M. Gibson, A.J. Sedman, E.L. Posvar, Multiple-dose pharmacokinetics, pharmacodynamics, and safety of atorvastatin, an inhibitor of HMG-CoA reductase, in healthy subjects, Clin. Pharmacol. Ther. 60 (1996) 687–695.
[4] H. Lennernas, Clinical pharmacokinetics of atorvastatin, Clin. Pharmacokinet. 42 (2003) 1141–1160.
[5] H. Shen, M. Zhong, Preparation and evaluation of self-microemulsifying drug delivery systems (SMEDDS) containing atorvastatin, J. Pharm. Pharmacol. 58 (2006) 1183–1191.
[6] B. Subramaniam, R.A. Rajewski, K. Snavely, Pharmaceutical processing with supercritical carbon dioxide, J. Pharm. Sci. 86 (1997) 885–890.
[7] F. Dehghani, N.R. Foster, Dense gas anti-solvent processes for pharmaceutical formulation, Curr. Opin. Solid State Mater. Sci. 7 (2003) 363–369.
[8] S. Lee, K. Nam, M.-S. Kim, S.W. Jun, J.-S. Park, J.S. Woo, S.-J. Hwang, Preparation and characterization of solid dispersions of itraconazole by using aerosol solvent extraction system for improvement in drug solubility and bioavailability, Arch. Pharm. Res. 28 (2005) 866–874.
[9] D.-H. Won, M.-S. Kim, S. Lee, J.-S. Park, S.-J. Hwang, Improved physicochemical characteristics of felodipine solid dispersion particles by supercritical anti-solvent precipitation process, Int. J. Pharm. 301 (2005) 199–208.
[10] I. Pasquali, R. Bettini, F. Giordano, Solid-state chemistry and particle engineering with supercritical fluids in pharmaceutics, Euro. J. Pharm. Sci. 27 (2006) 299–310.
[11] S.W. Jun, M.-S. Kim, J.-S. Kim, H.J. Park, S. Lee, J.-S. Woo, S.-J. Hwang, Preparation and characterization of simvastatin/hydroxypropyl-β-cyclodextrin inclusion complex using supercritical antisolvent (SAS) process, Euro. J. Pharm. Biopharm. 66 (2007) 413–421.
[12] E. Reverchon, Supercritical antisolvent precipitation of micro- and nano-particles, J. Supercrit. Fluids 15 (1999) 1–21.
[13] S.A. Shoyele, S. Cawthorne, Particle engineering techniques for inhaled biopharmaceuticals, Adv. Drug Deliv. Rev. 58 (2006) 1009–1029.
[14] A. Kordikowski, T. Shekunov, P. York, Polymorph control of sulfathiazole on supercritical CO_2, Pharm. Res. 18 (2001) 682–688.
[15] H.H. Tong, B.Y. Shekunov, P. York, A.H. Chow, Thermal analysis of trace levels of polymorphic impurity in salmeterol xinafoate samples, Pharm. Res. 20 (2003) 1423–1429.
[16] S.D. Yeo, J.C. Lee, Crystallization of sulfamethizole using the supercritical and liquid antisolvent processes, J. Supercrit. Fluids 30 (2004) 315–323.
[17] H.J. Park, M.-S. Kim, S. Lee, J.-S. Kim, J.-S. Woo, J.S. Park, S.J. Hwang, Recrystallization of fluconazole using supercritical antisolvent (SAS) process, Int. J. Pharm. 328 (2007) 152–160.
[18] A. Martin, P. Bustamante, A.H.C. Chun, Physical Pharmacy: Physical Chemical Principles in the Pharmaceutical Sciences, fourth ed., Lippincott Williams & Wilkins, Baltimore, 1993.
[19] M.-S. Kim, S. Lee, J.S. Park, J.-S. Woo, S.J. Hwang, Micronization of cilostazol using supercritical antisolvent (SAS) process, Powder Technol. 177 (2007) 64–70.
[20] E. Reverchon, I. De Marco, Supercritical antisolvent micronization of cefonicid: thermodynamic interpretation of results, J. Supercrit. Fluids 31 (2004) 207–215.
[21] E. Reverchon, I. De Marco, Supercritical antisolvent precipitation of cephalosporins, Powder Technol. 164 (2006) 139–146.
[22] S.-D. Yeo, S.-J. Park, J.-W. Kim, J.-C. Kim, Critical properties of carbon dioxide + methanol, + ethanol, + 1-propanol, and + 1-butanol, J. Chem. Eng. Data 45 (2000) 932–935.

[23] S.N. Joung, C.W. Woo, H.Y. Shin, S.Y. Kim, K.P. Yoo, C.S. Lee, W.S. Huh, Measurements and correlation of high-pressure VLE of binary CO_2–alcohol systems (methanol, ethanol, 2-methoxyethanol and 2-ethoxyethanol), Fluid Phase Equilib. 185 (2001) 219–230.
[24] J. Liu, Z. Qin, G. Wang, X. Hou, J. Wang, Critical properties of binary and ternary mixtures of hexane + methanol, hexane + carbon dioxide, methanol + carbon dioxide, and hexane + carbon dioxide + methanol, J. Chem. Eng. Data 48 (2003) 1610–1613.
[25] M. Mukhopadhyay, S.V. Dalvi, Mass and heat transfer analysis of SAS: effects of thermodynamic states and flow rates on droplet size, J. Supercrit. Fluids 30 (2004) 333–348.
[26] H. Krober, U. Teipel, Materials processing with supercritical antisolvent precipitation: process parameters and morphology of tartaric acid, J. Supercrit. Fluids 22 (2002) 229–235.
[27] M. Rantakylä, M. Jäntti, O. Aaltonen, M. Hurme, The effect of initial drop size on particle size in the supercritical antisolvent precipitation (SAS) technique, J. Supercrit. Fluids 24 (2002) 251–263.
[28] E.W. Lemmon, A.P. Peskin, M.O. McLinden, D.G. Friend, NIST thermodynamic and transport properties of pure fluids-NIST Standard Reference Database 12 (Version 5.0). Software package by NIST, US Department of Commerce. 2000.
[29] E. Reverchon, I. De Marco, G. Della Porta, Rifampicin microparticles production by supercritical antisolvent precipitation, Int. J. Pharm. 243 (2002) 83–91.
[30] Q.L. Suo, W.Z. He, Y.C. Huang, C.P. Li, H.L. Hong, Y.X. Li, M.D. Zhu, Micronization of the natural pigment-bixin by the SEDS process through prefilming atomization, Powder Technol. 154 (2005) 110–115.
[31] B. Warwick, F. Dehghani, N.R. Foster, J.R. Biffin, H.L. Regtop, Micronization of copper indomethacin using gas antisolvent processes, Ind. Eng. Chem. Res. 41 (2002) 1993–2004.
[32] E. Reverchon, I. De Marco, G. Della Porta, Tailoring of nano- and micro-particles of some superconductor precursors by supercritical antisolvent precipitation, J. Supercrit. Fluids 23 (2002) 81–87.
[33] S. Bristow, T. Shekunov, B.Y. Shekunov, P. York, Analysis of the supersaturation and precipitation process with supercritical CO_2, J. Supercrit. Fluids 21 (2001) 257–271.
[34] International Conference of Harmonization Q3C, Impurities: Residual Solvents, Federal Register 68, 64352–64353. 1997.
[35] G.E. Amidon, W.I. Higuchi, N.F. Ho, Theoretical and experimental studies of transport of micelle-solubilized solutes, J. Pharm. Sci. 71 (1982) 77–84.
[36] R.K. Khankary, D.J.W. Grant, Pharmaceutical hydrates, Thermochim. Acta 248 (1995) 61–79.
[37] M. Sugimoto, T. Okagaki, S. Narisawa, Y. Koida, K. Nakajima, Improvement of dissolution characteristics and bioavailability of poorly water-soluble drugs by novel cogrinding method using water-soluble polymer, Int. J. Pharm. 160 (1998) 11–19.
[38] K. Yamashita, T. Nakate, K. Okimoto, A. Ohike, Y. Tokunaga, R. Ibuki, K. Higaki, T. Kimura, Establishment of new preparation method for solid dispersion formulation of tacrolimus, Int. J. Pharm. 267 (2003) 79–91.
[39] J.M. Vaughn, J.T. McConville, M.T. Crisp, K.P. Johnston, R.O. Williams III, Supersaturation produces high bioavailability of amorphous danazol particles formed by evaporative precipitation into aqueous solution and spray freezing into liquid technologies, Drug Dev. Ind. Pharm. 32 (2006) 559–567.